Received: 8 March 2022 | Revised: 23 April 2022 | Accepted: 29 May 2022

DOI: 10.1111/cas.15456

ORIGINAL ARTICLE

Cancer Science WILEY

Mutation profiles in circulating cell-free DNA predict acquired resistance to olaparib in high-grade serous ovarian carcinoma

Dianxing Hu[1] | Ensong Guo[1] | Bin Yang[1] | Xu Qin[2] | Yu Fu[1] | Junpeng Fan[1] | Xucui Zhuang[1] | Qianqian Yao[3] | Funian Lu[1] | Wenting Li[1] | Rourou Xiao[1] | Xue Wu[1] | Xiaohang Yang[1] | Zizhuo Wang[1] | Chen Liu[1] | Lixin You[1] | Rongyu Zang[4] | Qi Zhou[5] | Weidong Zhao[6] | Gang Chen[1] | Chaoyang Sun[1]

[1]Department of Obstetrics and Gynecology, Tongji Hospital, Tongji Medical College, Huazhong University of Science and Technology, Wuhan, China

[2]Department of Stomatology, Tongji Hospital, Tongji Medical College, Huazhong University of Science and Technology, Wuhan, China

[3]Department of Medical Science, Shanghai AccuraGen Biotechnology Co., Ltd., Shanghai, China

[4]Department of Gynecologic Oncology, Zhongshan Hospital, Fudan University, Shanghai, China

[5]Department of Gynecologic Oncology, Chongqing University Cancer Hospital, Chongqing, China

[6]Department of Gynecologic Oncology, Anhui Provincial Cancer Hospital, Hefei, China

Correspondence
Chaoyang Sun, Department of Obstetrics and Gynecology, Tongji Hospital, Tongji Medical College, Huazhong University of Science and Technology, No. 1095 Jiefang Avenue, Wuhan, 430030 Hubei, China.
Email: suncydoctor@gmail.com

Funding information
National Natural Science Foundation of China, Grant/Award Number: 81874106, 81974408, 82073259, 82103065; Key Research and Development Program of Hubei Province, Grant/Award Number: 2020BCA067; Hubei Province Science Fund for Distinguished Young Scholars, Grant/Award Number: 2020CFA066

Abstract

Although resistance to poly(ADP-ribose) polymerase inhibitors (PARPi) has gradually become a major challenge in the maintenance therapy for high-grade serous ovarian carcinoma (HGSOC), there are no universal indicators for resistance monitoring in patients. A key resistance mechanism to PARPi is the restoration of homologous recombination repair (HRR), including *BRCA* reversion mutations and changes in DNA damage repair proteins. To explore mutation profiles associated with PARPi resistance, we undertook targeted 42-gene deep sequencing of circulating cell-free DNA (cfDNA) extracted from HGSOC patients pre- and post-treatment with olaparib maintenance therapy. We found that pathogenic germline mutations in the HRR pathway, including *BRCA1/2*, were strongly associated with improved clinical outcomes, and newly acquired *MRE11A* mutations significantly shortened the progression-free survival (PFS) of patients. Furthermore, dynamic fluctuations of somatic mutation sites in *CHEK2*:*p.K373E* and *CHEK2*:*p.R406H* can be used for evaluating the therapeutic efficacy of patients. *MRE11A*:*p.K464R* might be a vital driving factor of olaparib resistance, as patients with newly acquired *MRE11A*:*p.K464R* in post-treatment cfDNA had significantly shorter PFS than those without it. These findings provide potential noninvasive biomarkers for efficacy evaluation and resistance monitoring of olaparib

Abbreviations: cfDNA, cell-free DNA; CLAmp-seq, circular ligation amplification and sequencing; DDR, DNA damage repair; gBRCA, germline *BRCA1/2*; gDNA, genomic DNA; HGSOC, high-grade serous ovarian carcinoma; HRR, homologous recombination repair; MAF, mutant allele frequency; Max MAF, maximum mutant allele frequency; NGS, next-generation sequencing; PARP, poly(ADP-ribose) polymerase; PARPi, poly(ADP-ribose) polymerase inhibitor; PB, peripheral blood; PFS, progression-free survival; WBC, white blood cell.

treatment, and lay the foundation for developing combination treatment after olaparib resistance.

KEYWORDS
biomarker, cfDNA, HGSOC, mutation profile, PARP inhibitor resistance

1 | INTRODUCTION

High-grade serous ovarian carcinoma is the most common pathological type of ovarian epithelial tumor. Its tumorigenesis is generally asymptomatic and early diagnosis is difficult, resulting in approximately 75% of patients being diagnosed at advanced stage. In addition, HGSOC patients are more likely to relapse and develop drug resistance after treatment; the 5-year survival rate of patients with advanced disease is less than 30%.[1] Therefore, clinical experts have been looking for ways to reduce relapse and improve patients' prognosis.

Poly(ADP-ribose) polymerase inhibitors open a new chapter in maintenance therapy of HGSOC patients. When the HRR pathway is disrupted, such as *BRCA1/2* mutations, tumor cells will produce homologous recombination deficiency and form a synthetic lethal effect with PARPi.[2,3] Olaparib, as a representative of PARPi, has been mainly used in maintenance therapy of platinum-sensitive ovarian cancer patients,[4,5] and it has provided significant long-term survival benefit in clinical studies at home and abroad. However, with the widespread application of olaparib, its drug resistance is becoming increasingly prominent. Mounting evidence has suggested that PARPi resistance is closely related to HRR restoration, including *BRCA1/2* reversion mutations and changes in DDR proteins (e.g., ATM, 53BP1, RAD51, and CDK12).[6–9] Moreover, our previous study showed that acquired *KRAS* mutation or mutations of other components of the MAPK pathway lead to primary and acquired PARPi resistance.[10] Therefore, exploring a viable method for monitoring molecular changes of HGSOC patients will contribute to solving the clinical dilemma of olaparib resistance.

Cell-free DNA analysis can achieve continuous and repeatable monitoring of tumor molecular characterizations at different stages of diagnosis and treatment in patients.[11,12] Cell-free DNA analysis has gradually highlighted its technical advantages in clinical practice, such as risk stratification, response assessment, and resistance monitoring.[13] For example, it can predict the risk of postoperative recurrence of colorectal cancer,[14] guide the application of targeted therapy in non-small-cell lung cancer,[15,16] and screen prostate cancer patients who benefit from PARPi treatment.[17] Similarly, *BRCA* reversion mutations detected by cfDNA can predict primary or acquired resistance to rucaparib in HGSOC patients,[18] suggesting that cfDNA analysis could be an effective means for efficacy evaluation and resistance monitoring of olaparib.

In this study, we investigated the development of genetic resistance to olaparib in a retrospective study using sequential cfDNA sampling in platinum-sensitive HGSOC patients. We identified the cfDNA mutation profiles, determined the correlations between cfDNA mutation profiles and patient prognosis, and screened out mutation biomarkers and potential drug targets in HGSOC patients with olaparib resistance.

2 | MATERIALS AND METHODS

2.1 | Collection of samples and clinical information

Peripheral blood samples (10 ml) were collected using LBgard Blood Tubes (Biomatrica) prior to olaparib treatment and at later follow-ups (every 3 months until 12 months after treatment) in patients. Healthy subjects were recruited to collect 10 ml PB samples as the baseline for cfDNA analysis. Clinical information from patients was collected for subsequent analysis.

2.2 | Peripheral blood sample processing

All PB samples were processed within 3–4 days, including sample collection, transportation, and separation of blood components. The separation process was carried out as follows. First, unqualified PB samples with coagulation or hemolysis were excluded. Next, PB samples were centrifuged at 1600 *g* for 10 min at 4°C to separate plasma and WBC. Plasma was transferred into a new 2 ml microcentrifuge tube, followed by centrifugation at 16,000 *g* for 10 min at 4°C to remove any remaining cellular components. Plasma was then transferred into a new 2 ml microcentrifuge tube for cfDNA extraction. White blood cells were collected using a new 2 ml microcentrifuge tube for isolating gDNA. All plasma and WBC were immediately stored at −80°C until DNA extraction. Sample processing time did not exceed 1 h.

2.3 | Genomic DNA extraction

Genomic DNA was extracted from 100 μl WBC using the TIANamp Blood DNA Kit (Tiangen) following the manufacturer's instructions and was quantified by a Nanodrop 2000 spectrophotometer (Thermo Fisher Scientific). Quality control was as follows: concentration >1 ng/μl and no protein or RNA contamination. Extracted gDNA was stored at −80°C until sequencing.

2.4 | Cell-free DNA extraction

Cell-free DNA was extracted from 4 ml plasma using the QIAamp Circulating Nucleic Acid Kit (Qiagen) in accordance with the manufacturer's instructions. Extracted cfDNA was quantified by a Qubit 3.0 fluorometer (Life Technologies) and 2100 Electrophoresis Bioanalyzer Instrument (Agilent Technologies). Quality control was as follows: (i) a typical peak around 167 bp, (ii) no obvious gDNA contamination, and (iii) total content >10 ng. Extracted cfDNA was stored at −80°C until sequencing.

2.5 | Library construction and sequencing

The gDNA was sonicated into short fragments using a Covaris ultrasonicator, with the peak around 200 bp. The linear cfDNA molecules were denatured and circularized to form templates for rolling circle amplification reaction. Next, 100 ng fragmented gDNA and amplified cfDNA were used for library construction using the KAPA sequencing library construction kit (Kapa Biosystems) following the manufacturer's instructions. Sequencing libraries were captured by a 42-gene panel, followed by sequencing on an Illumina HiSeq 2500. The sequencing scheme of 250 paired ends was used to obtain the full sequence information. Unique sequencing reads were determined by the AccuraGen proprietary algorithm. The average coverage depth for all probes was approximately 690× in gDNA and 68,014× in cfDNA. Cell-free DNA samples from healthy subjects were detected following the procedure described above.

2.6 | Sequencing data processing

The variants of gDNA and cfDNA were called using AccuraGen's NGS pipeline (AccuraGen Biotechnology Co., Ltd.). Briefly, sequencing reads were aligned to the hg19/GRCh37 reference genome by the Burrows–Wheeler Alignment tool (http://bio-bwa.sourceforge.net/bwa.shtml). Duplicate removal were carried out using SAMBLASTER[19] followed by single nucleotide polymorphism and indel calling using FreeBayes.[20] Variants in low-complexity regions were removed and annotated using GEMINI.[21] In addition, background noise introduced by random NGS error was removed by the AccuraGen proprietary algorithm and cfDNA sequencing data from healthy subjects was used as the baseline for cfDNA analysis. Somatic mutations were determined by cross-checking cfDNA sequencing data with germline and clonal hematopoietic variants from gDNA. Mutant allele frequency was calculated by comparing the variant reads to total sequencing reads of the variant site.

2.7 | Statistical analysis

Pearson correlation analysis was used to assess correlations between different parameters. Unpaired or paired *t*-test was used for comparison between two groups, and ordinary one-way ANOVA was used for comparison among three groups. The differences between the proportions of two or three groups were analyzed by χ^2-test and Kruskal–Wallis test with Dunn's multiple comparisons test, respectively. Log–rank (Mantel–Cox) test was utilized to determine the differences in survival curves. The above analyses were undertaken using GraphPad Prism 7 (GraphPad Software). Results were considered statistically significant when $p < 0.05$.

3 | RESULTS

3.1 | Procedure for cfDNA analysis in HGSOC patients

This work was carried out retrospectively on prospectively collected samples from platinum-sensitive HGSOC patients with olaparib maintenance therapy. Peripheral blood samples from 25 HGSOC patients and 37 healthy subjects were collected for cfDNA analysis and baseline detection, respectively (Figure 1). The clinical characteristics of patients are described in Table 1. Cell-free DNA was extracted from plasma samples collected from patients (Figure 1A, B0–B4) and healthy subjects. A personalized panel containing 42 genes was customized to detect germline and somatic mutations (Table S1). Circular ligation amplification and sequencing[22] was used for mutation detection (Figure 1B,C), in which gDNA of B0 samples were used to identify germline mutations, and 96 cfDNA (35 healthy subject-derived and 61 patient-derived) samples were detected for analyzing somatic mutations in patients (Figure 1B). For data processing, we estimated tumor load in cfDNA using Max MAF.[23,24] Variant-supporting reads >2 and without germline mutations were defined as the criteria for somatic mutations.

3.2 | Dynamic changes of Max MAF are associated with prognosis of olaparib maintenance therapy

By integrating the follow-up information of patients, we plotted the distribution maps of PFS, cfDNA yield, and Max MAF in pretreatment patients (Figure 2A), and analyzed the correlations between them. We found that Max MAF was significantly positively correlated with PFS relative to cfDNA yield (Figure 2B,C). Moreover, Max MAF was significantly increased in post-treatment patients, suggesting that it could play an important role in affecting the prognosis of olaparib treatment, but cfDNA yield did not (Figure 2D,E). Next, we plotted the dynamic changes of cfDNA or Max MAF with treatment progress under different outcomes, and observed that the worse the patients' prognosis, the higher the proportion of patients with increased Max MAF, in which the proportion of "Relapsed < 12 m" even reached 100% (Figure 2F). We then compared the fluctuations of cfDNA or Max MAF and CA125 levels during olaparib treatment, respectively, and found that cfDNA yield did not show a consistent trend with CA125 (Figure S1A–C). For Max MAF, although the

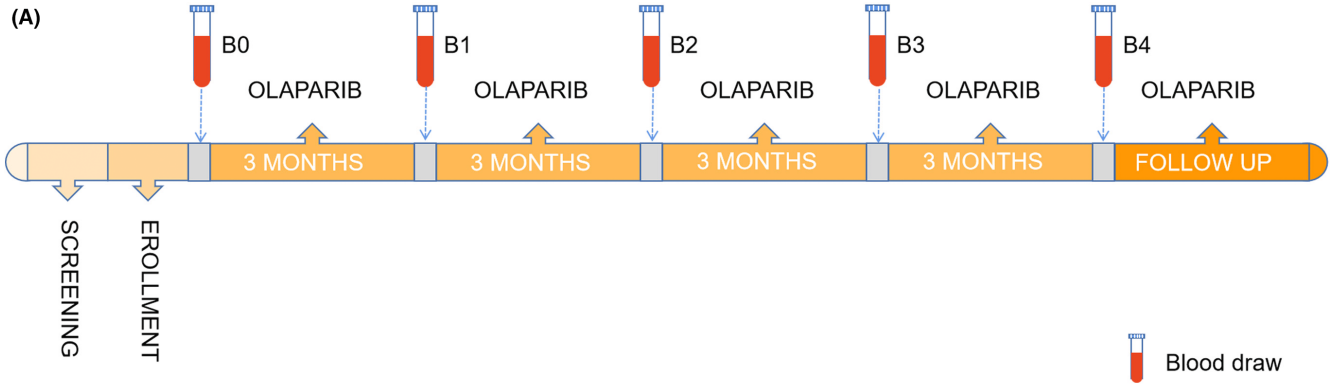
(A)
B0
B1
B2
B3
B4
OLAPARIB
OLAPARIB
OLAPARIB
OLAPARIB
OLAPARIB
3 MONTHS
3 MONTHS
3 MONTHS
3 MONTHS
FOLLOW UP
SCREENING
EROLLMENT
Blood draw

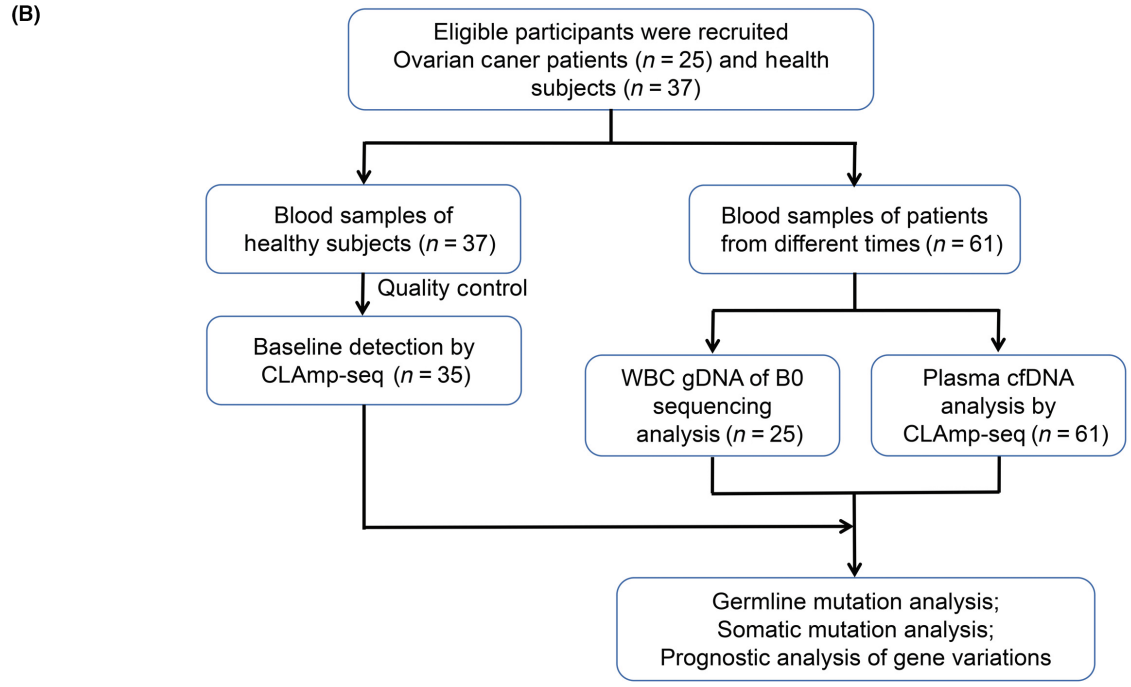
(B)
Eligible participants were recruited
Ovarian caner patients (n = 25) and health subjects (n = 37)
Blood samples of healthy subjects (n = 37)
Quality control
Baseline detection by CLAmp-seq (n = 35)
Blood samples of patients from different times (n = 61)
WBC gDNA of B0 sequencing analysis (n = 25)
Plasma cfDNA analysis by CLAmp-seq (n = 61)
Germline mutation analysis;
Somatic mutation analysis;
Prognostic analysis of gene variations

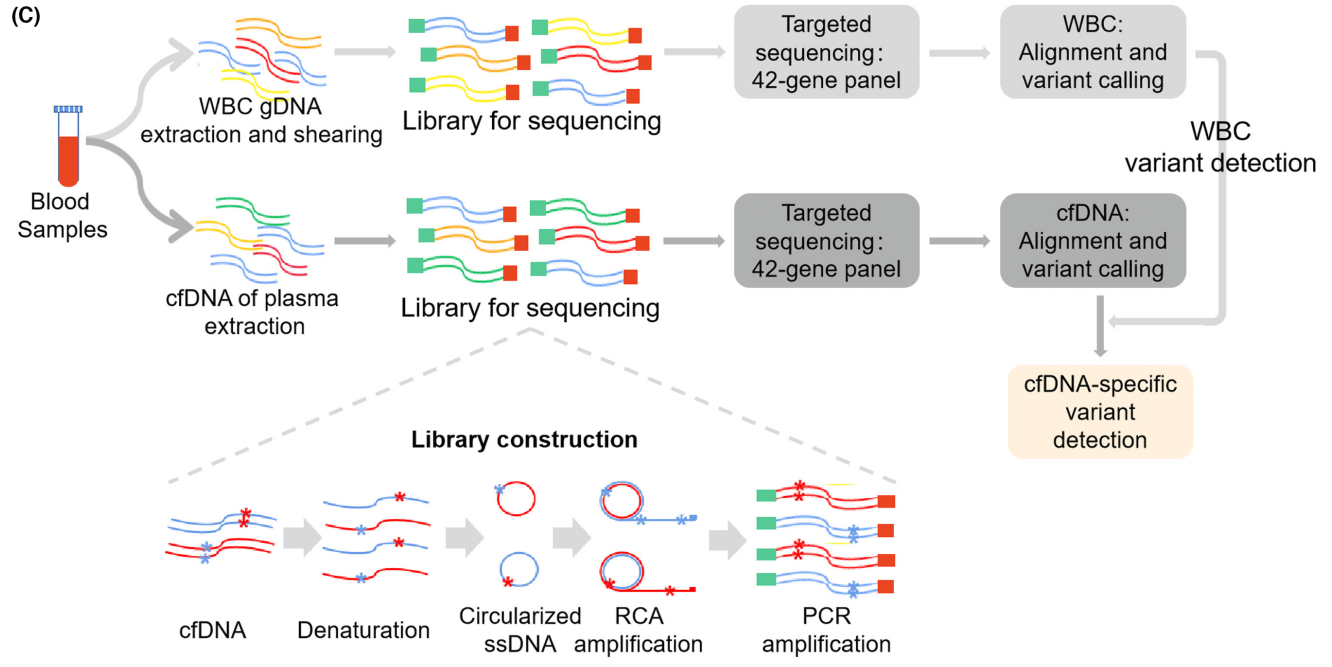
(C)
Blood Samples
WBC gDNA extraction and shearing
Library for sequencing
Targeted sequencing: 42-gene panel
WBC: Alignment and variant calling
WBC variant detection
cfDNA of plasma extraction
Library for sequencing
Targeted sequencing: 42-gene panel
cfDNA: Alignment and variant calling
cfDNA-specific variant detection
Library construction
cfDNA
Denaturation
Circularized ssDNA
RCA amplification
PCR amplification

FIGURE 1 Study schema and method for cell-free DNA (cfDNA) analysis in patients with high-grade serous ovarian carcinoma. (A) Diagram showing the schema of peripheral blood (PB) sample collection. PB samples are collected at the following time points: pretreatment (B0), then every 3 months after olaparib treatment (B1, B2, B3, and B4). The duration of PB collection is determined according to the follow-up of patients. (B) Flow diagram showing the processing, detection, and analysis of cfDNA. C, Schema of the method of cfDNA detection. CLAmp-seq, circular ligation amplification and sequencing; gDNA, genomic DNA; RCA, rolling circle amplification; WBC, white blood cell

TABLE 1 Demographics of our cohort of patients with high-grade serous ovarian carcinoma treated with olaparib

	All ($n = 25$)	Unrelapsed ($n = 6$)	Relapsed ($n = 19$)
Age, years	53.24 (41–66)	51.83 (45–65)	53.68 (41–66)
Stage			
II	3	0	3
III	16	3	13
IV	6	3	3
NACT			
Y	3	1	2
N	22	5	17
Number of chemotherapy regimens			
2	15	4	11
≥2	10	2	8
Metastasis (enrollment)			
Y	14	3	11
N	11	3	8
Cytoreductive surgery (enrollment)			
Y	11	3	8
N	14	3	11
Response of chemotherapy regimens (enrollment)			
CR	11	3	8
PR	14	3	11
Pathogenic germline mutations of *BRCA*			
Y	8	3	5
N	17	3	14
Somatic mutations of *BRCA*			
Y	4	1	3
N	21	5	16
Benign mutations of *BRCA*			
≤3	7	2	5
3 < No. ≤5	7	1	6
>5	11	3	8
Somatic mutations of *TP53*			
Y	11	2	9
N	14	4	10

Abbreviations: *BRCA*, including *BRCA1* and *BRCA2*; CR, complete response; N, No; NACT, new adjuvant chemotherapy treatment; PR, partial response; Y, Yes.

changes of Max MAF and CA125 were irregular in the "Unrelapsed" group (Figure S1D), their fluctuations tended to be consistent in the relapsed patients, especially in the "Relapsed < 12 m" group (Figure S1E,F). Furthermore, there was a significant difference in the trend of proportional changes in increasing cfDNA yield and Max MAF (Figure 2G). These results suggested that increased Max MAF in post-treatment could predict the patients' relapse.

To validate the effect of Max MAF on patients' prognosis, we plotted the survival curves and found increased Max MAF was significantly associated with poor prognosis of patients (Figure 2I), but cfDNA yield was not (Figure 2H). It confirmed the feasibility of monitoring olaparib resistance by Max MAF detection.

3.3 | Pathogenic germline mutations of HRR pathway influence the prognosis of olaparib maintenance therapy

The defects of the HRR pathway can form a synthetic lethal effect with PARPi in ovarian cancer.[2] Therefore, we plotted a germline mutation map and screened out pathogenic or likely pathogenic mutations (pathogenic mutations) in patients (Figure 3A,B). Furthermore, we found that the whole mutation load had no effect on patients' outcomes (Figure 3C,D), but patients with pathogenic mutations had significant survival benefits compared to those without them (Figure 3E,F), highlighting the effectiveness of synthetic lethal effect in clinical practice.

Considering the high proportion of pathogenic gBRCA mutations, we analyzed and found that patients with gBRCA mutations had a degree of survival advantage (Figure 3G,H). These results suggested that HRR-related pathogenic germline mutations in HGSOC patients affected the efficacy of olaparib maintenance therapy and were closely related to patients' prognosis.

3.4 | Somatic mutations under pathogenic germline mutations are associated with prognosis of olaparib maintenance therapy

We further plotted the distribution maps of somatic mutations in patients with pathogenic germline mutations (Figure S2A–C) and observed that high-frequency (≥3) mutations of *CHEK2*, *TP53*, *MRE11A*, and *ATM* in pretreatment (Figure S2B) and post-treatment (Figure S2C). Next, we explored their effect on patients' PFS by survival analysis. The results showed that patients with new *MRE11A* mutations in post-treatment had an extremely poor prognosis, with significantly shorter PFS compared to noncarriers (Figure S2I). However, no differences in PFS were observed for other high-frequency mutations or new mutations, including *TP53*, *MRE11A*, and *ATM* in pretreatment (Figure S2E–G) and *CHEK2* (Figure S2H), *ATM* (Figure S2J), and *TP53* (Figure S2K) in post-treatment.

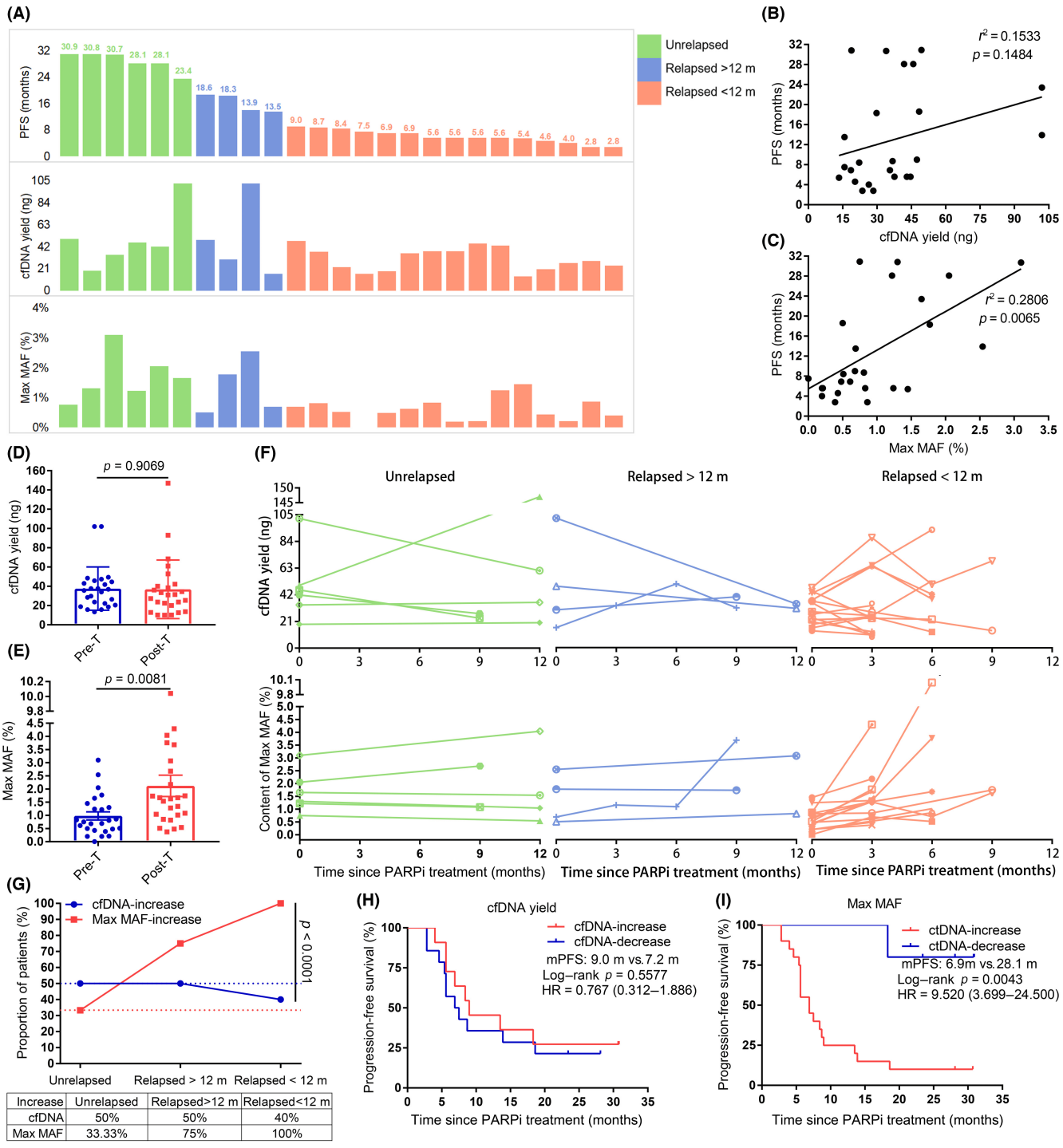

Increase	Unrelapsed	Relapsed>12 m	Relapsed<12 m
cfDNA	50%	50%	40%
Max MAF	33.33%	75%	100%

FIGURE 2 Associations between cell-free DNA (cfDNA) or maximum mutant allele frequency (Max MAF) and the prognosis of patients with high-grade serous ovarian carcinoma. (A) Distribution maps of progression-free survival (PFS), cfDNA yield, and Max MAF in pretreatment (B0). (B, C) Pearson correlation analysis between PFS and cfDNA yield (B, $p = 0.1484$) or Max MAF (C, $p = 0.0065$) at baseline (B0). (D, E) Differences of cfDNA yield (D, $p = 0.9069$) or Max MAF (E, $p = 0.0081$) in patients before treatment (Pre-T) and after treatment (Post-T), paired *t*-test. (F) Dynamic changes of cfDNA yield or Max MAF with treatment process in different outcomes. (G) Difference of the tendency of the proportion of increased cfDNA yield or Max MAF in different outcomes; χ^2-test, $p < 0.0001$. (H, I) Survival analyses of the changes of cfDNA yield (H, $p = 0.5577$) and Max MAF (I, $p = 0.0043$) in patients. HR, hazard ratio; mPFS, median PFS; PARPi, poly(ADP-ribose) polymerase inhibitor

Furthermore, we observed that high-frequency (≥3) new mutations were mainly concentrated in *MRE11A:p.K464R* (Figure S2D). Therefore, we explored its role in patients' prognosis and found that newly acquired *MRE11A:p.K464R* was strongly associated with poor prognosis of patients (Figure S2L). It revealed that *MRE11A:p.K464R* could be a reliable indicator for resistance monitoring of olaparib in HGSOC patients with pathogenic germline mutations.

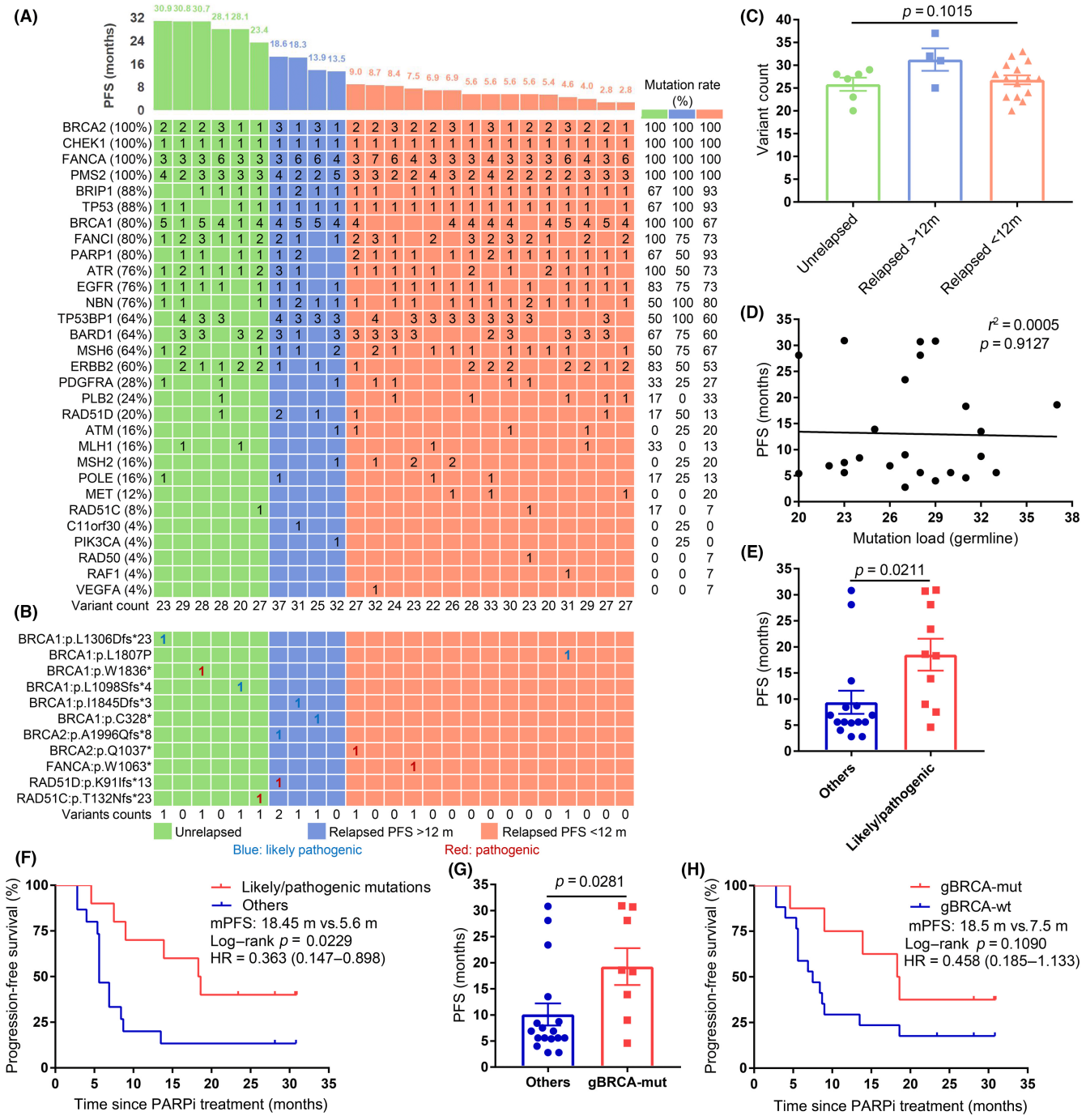

FIGURE 3 Pathogenic germline mutations of homologous recombination repair pathway improve the survival benefits of patients with high-grade serous ovarian carcinoma (HGSOC). (A) Germline mutation map of HGSOC patients at baseline (B0). (B) Distribution map of pathogenic germline mutations in patients at baseline (B0). (C) Differences in variant counts among different outcomes; ordinary one-way ANOVA, $p = 0.1015$. (D) Pearson correlation analysis between progression-free survival (PFS) and germline mutation load; $p = 0.9127$. (E) Differences in PFS between carriers and noncarriers of pathogenic mutations; unpaired *t*-test, $p = 0.0211$. (F) Survival analysis in patients with pathogenic germline mutations; $p = 0.0229$. (G) Differences in PFS between carriers and noncarriers of germline *BRCA1/2* (gBRCA) mutations; unpaired *t*-test, $p = 0.0281$. (H) Survival analysis in patients with gBRCA mutations (H, $p = 0.1090$). (C, E, G) Data are presented as mean ± SEM. HR, hazard ratio; mPFS, median PFS; PARPi, poly(ADP-ribose) polymerase inhibitor

3.5 | Somatic mutations in cfDNA influence the prognosis of olaparib maintenance therapy

Based on the above analyses, we realized that somatic mutations could be a more universal indicator for efficacy evaluation or resistance monitoring of olaparib maintenance therapy. Therefore, we plotted somatic mutation maps in cfDNA. As shown in Figure 4A,B, 80% (20/25) of patients had an increased mutation load, and 96% (24/25) of patients developed new mutations. Next, we compared the differences of somatic mutation load in patients

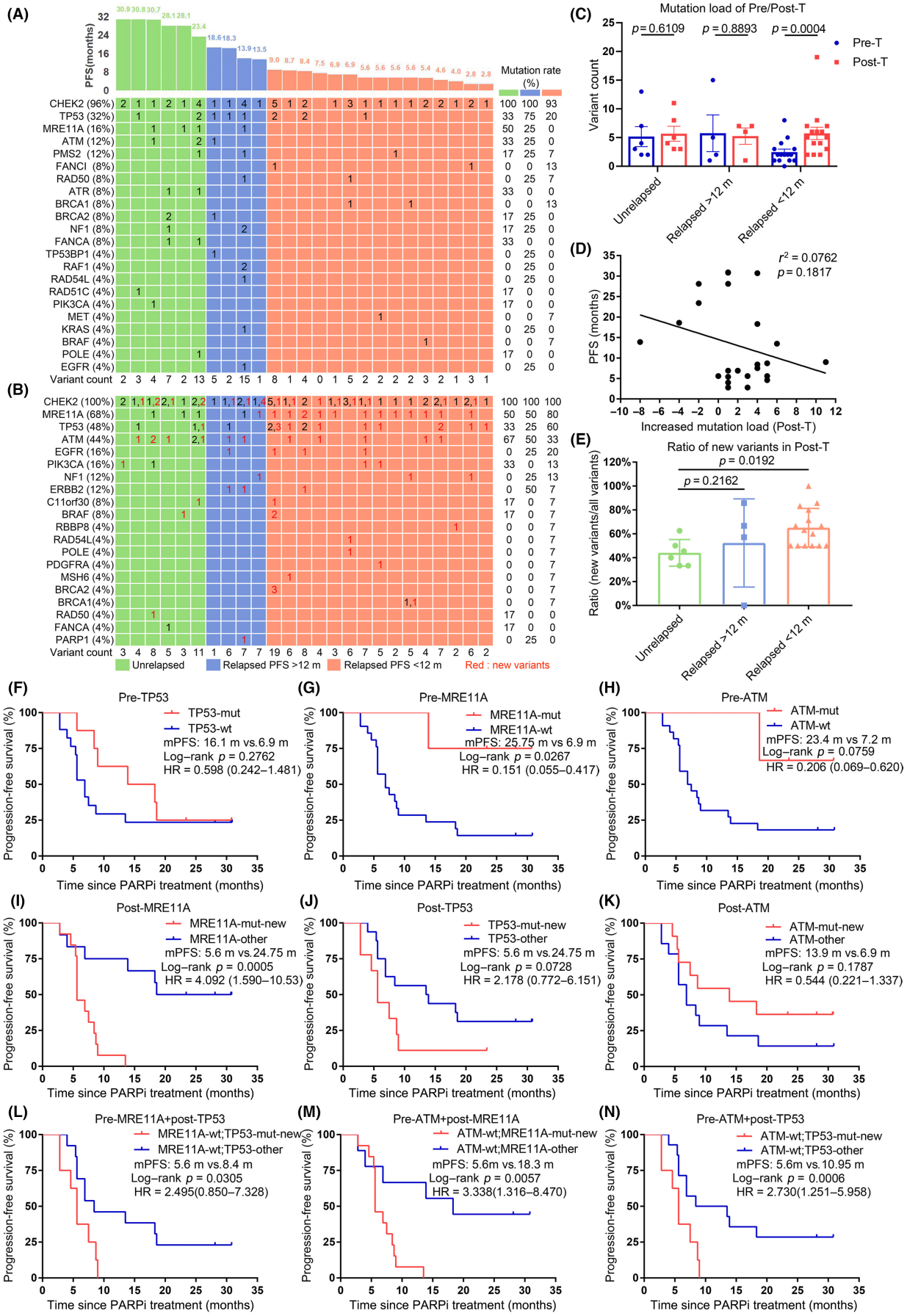
(A)
PFS(months)
Mutation rate (%)
CHEK2 (96%)
TP53 (32%)
MRE11A (16%)
ATM (12%)
PMS2 (12%)
FANCI (8%)
RAD50 (8%)
ATR (8%)
BRCA1 (8%)
BRCA2 (8%)
NF1 (8%)
FANCA (8%)
TP53BP1 (4%)
RAF1 (4%)
RAD54L (4%)
RAD51C (4%)
PIK3CA (4%)
MET (4%)
KRAS (4%)
BRAF (4%)
POLE (4%)
EGFR (4%)
Variant count
(B)
CHEK2 (100%)
MRE11A (68%)
TP53 (48%)
ATM (44%)
EGFR (16%)
PIK3CA (16%)
NF1 (12%)
ERBB2 (12%)
C11orf30 (8%)
BRAF (8%)
RBBP8 (4%)
RAD54L(4%)
POLE (4%)
PDGFRA (4%)
MSH6 (4%)
BRCA2 (4%)
BRCA1(4%)
RAD50 (4%)
FANCA (4%)
PARP1 (4%)
Variant count
Unrelapsed
Relapsed PFS >12 m
Relapsed PFS <12 m
Red : new variants
(C)
Mutation load of Pre/Post-T
p=0.6109
p=0.8893
p=0.0004
Pre-T
Post-T
Variant count
Unrelapsed
Relapsed >12 m
Relapsed <12 m
(D)
r² = 0.0762
p=0.1817
PFS (months)
Increased mutation load (Post-T)
(E)
Ratio of new variants in Post-T
p=0.0192
p=0.2162
Ratio (new variants/all variants)
Unrelapsed
Relapsed >12 m
Relapsed <12 m
(F)
Pre-TP53
TP53-mut
TP53-wt
mPFS: 16.1 m vs.6.9 m
Log–rank p = 0.2762
HR = 0.598 (0.242–1.481)
Progression-free survival (%)
Time since PARPi treatment (months)
(G)
Pre-MRE11A
MRE11A-mut
MRE11A-wt
mPFS: 25.75 m vs 6.9 m
Log–rank p = 0.0267
HR = 0.151 (0.055–0.417)
(H)
Pre-ATM
ATM-mut
ATM-wt
mPFS: 23.4 m vs 7.2 m
Log–rank p = 0.0759
HR = 0.206 (0.069–0.620)
(I)
Post-MRE11A
MRE11A-mut-new
MRE11A-other
mPFS: 5.6 m vs.24.75 m
Log–rank p = 0.0005
HR = 4.092 (1.590–10.53)
(J)
Post-TP53
TP53-mut-new
TP53-other
mPFS: 5.6 m vs.24.75 m
Log–rank p = 0.0728
HR = 2.178 (0.772–6.151)
(K)
Post-ATM
ATM-mut-new
ATM-other
mPFS: 13.9 m vs.6.9 m
Log–rank p = 0.1787
HR = 0.544 (0.221–1.337)
(L)
Pre-MRE11A+post-TP53
MRE11A-wt;TP53-mut-new
MRE11A-wt;TP53-other
mPFS: 5.6 m vs.8.4 m
Log–rank p = 0.0305
HR = 2.495(0.850–7.328)
(M)
Pre-ATM+post-MRE11A
ATM-wt;MRE11A-mut-new
ATM-wt;MRE11A-other
mPFS: 5.6m vs.18.3 m
Log–rank p = 0.0057
HR = 3.338(1.316–8.470)
(N)
Pre-ATM+post-TP53
ATM-wt;TP53-mut-new
ATM-wt;TP53-other
mPFS: 5.6m vs.10.95 m
Log–rank p = 0.0006
HR = 2.730(1.251–5.958)

FIGURE 4 Associations between somatic mutation profiles and the prognosis of olaparib maintenance therapy in patients with high-grade serous ovarian carcinoma. (A, B) Distribution maps of somatic mutations in pretreatment (Pre-T) (A) and post-treatment (Post-T) (B) patients. (C) Changes of mutation load in patients before and after olaparib treatment. Paired *t*-test: Unrelapsed, $p = 0.6109$; Relapsed > 12 months, $p = 0.8893$; Relapsed < 12 months, $p = 0.0004$. (D) Pearson correlation analysis between progression-free survival (PFS) and increased mutation load in post-treatment; $p = 0.1817$. (E) Differences in the ratio of new mutations among different outcomes. Kruskal–Wallis test with Dunn's multiple comparisons test: Unrelapsed versus Relapsed > 12 months, $p = 0.2162$; Unrelapsed versus Relapsed < 12 months, $p = 0.0192$. (F–H) Survival analyses of somatic mutations (mut) in *TP53* (F, $p = 0.2762$), *MRE11A* (G, $p = 0.0267$), and *ATM* (H, $p = 0.0759$) in Pre-T patients. (I–K) Survival analyses of new somatic mutations in *MRE11A* (I, $p = 0.0005$), *TP53* (J, $p = 0.0728$), and *ATM* (K, $p = 0.1787$) in Post-T patients. (L–N) Survival analyses of combined somatic mutations of pre-*MRE11A* + post-*TP53* (L, $p = 0.0305$), pre-*ATM* + post-*MRE11A* (M, $p = 0.0057$), and pre-*ATM* + post-*TP53* (N, $p = 0.0006$) in patients. (C, E) Data are presented as mean ± SEM. HR, hazard ratio; mPFS, median PFS; PARPi, poly(ADP-ribose) polymerase inhibitor

before and after olaparib treatment among different outcomes, and found that increased somatic mutation load in post-treatment predicted a poor prognosis (Figure 4C) and has a negative correlation trend with patients' PFS (Figure 4D). In addition, the higher ratio of new somatic mutations in total mutation load, the worse patients' prognosis (Figure 4E), indicating that it might be a crucial factor for olaparib resistance in HGSOC patients.

Next, we summarized all high-frequency (≥3) somatic mutations in cfDNA (Table S2), and analyzed their impact on patients' prognosis. Due to the extremely high frequency of *CHEK2* in pretreatment (96%) and post-treatment (100%) (Figure 4A,B), we only analyzed the role of new *CHEK2* mutations in patients' prognosis, but no meaningful result was observed (Figure S3B). For other somatic mutations, compared with *TP53* (Figure 4F) and *PMS2* (Figure S3A), *MRE11A* mutations could significantly prolong patients' PFS in pretreatment (Figure 4G). Similarly, *ATM* mutations also tended to improve patients' prognosis (Figure 4H). In post-treatment, we unexpectedly observed the opposite effect of new *MRE11A* mutations compared with pretreatment, which significantly shortened the PFS of patients, indicating a strong correlation with olaparib resistance (Figure 4I). We also found that new *TP53* and *ATM* mutations had opposite trends in their impacts on patients' prognosis (Figure 4J,K). However, new mutations of *EGFR*, *PIK3CA*, *NF1*, and *ERBB2* did not affect patients' PFS (Figure S3C–F).

Furthermore, we evaluated the combined effect of somatic mutations on patients' prognosis and observed that the combination of pre-*MRE11A* + post-*TP53* significantly differentiated patients' prognosis (Figure 4L). Pre-*ATM* combined with post-*MRE11A* or post-*TP53* also shortened patients' PFS (Figure 4M,N). However, we found that only the combination of pre-*ATM* + post-*TP53* greatly improved the efficiency of prognostic assessment (Figure 4N). In addition, although the combination of *MRE11A* mutations with other somatic mutations distinguished patients' PFS well, the efficiency was significantly reduced compared with *MRE11A* alone (Figures 4L,M and S3G–I), revealing the specificity and reliability of *MRE11A* mutations as an indicator for efficacy evaluation and resistance monitoring of olaparib.

3.6 | Somatic mutation sites in cfDNA are associated with the prognosis of olaparib maintenance therapy

We have confirmed that somatic mutations in cfDNA were closely related to patients' prognosis. To better elucidate their role in disease progression, we further summarized the somatic mutation sites in cfDNA (Table S3) and analyzed the relationships between high-frequency (≥3) mutation sites and patients' prognosis. We first plotted the distribution maps of mutation sites, and found that *CHEK2:p.K373E* and *CHEK2:p.R406H* had no new mutations in post-treatment (Figure 5A,B). In contrast, the proportion of newly acquired *MRE11A:p.K464R* was up to 52% (13/25), and contributed 92.9% (13/14) of new mutation load in *MRE11A* (Figure 5B). Furthermore, we observed *CHEK2:p.K373E* and *MRE11A:p.K464R* in pretreatment significantly prolonged the PFS of patients (Figure 5C,E), whereas *CHEK2:p.R406H* did not (Figure 5D).

In post-treatment, we drew the dynamic curves of *CHEK2:p.K373E* and *CHEK2:p.R406H* during the sampling period, and observed that the content of them increased in relapsed patients (Figure 5F,G). We also plotted the relationships between their fluctuations and disease progression in all patients. The results showed that the proportion of disease progression in patients with increased *CHEK2:p.K373E* and *CHEK2:p.R406H* ("higher") was as high as 66.7% (10/15) and 100% (9/9), respectively (Figure S4A,B). Survival analysis also confirmed that increased *CHEK2:p.K373E* and *CHEK2:p.R406H* predicted a poor prognosis (Figure 5H,I). In addition, their combined effect was only observed to distinguish the prognosis of patients in post-treatment, and the efficiency was not improved relative to *CHEK2:p.R406H* alone (Figure S4C,D).

For *MRE11A:p.K464R*, its fluctuation in relapsed patients came from newly acquired mutations (Figure 5B,J). By analyzing the dynamic changes of *MRE11A:p.K464R* in all patients, we were surprised to find that once patients acquired the *MRE11A:p.K464R*, it often predicted disease progression or drug resistance, with the proportion as high as 92.3% (12/13). In contrast, only 25% (3/12) of patients with *MRE11A:p.K464R* in pre-existing or negative groups developed disease progression (Figure 5K). As expected, newly acquired *MRE11A:p.K464R* greatly shortened patients' PFS, suggesting that it plays a vital role in olaparib resistance (Figure 5L). Furthermore, we analyzed the role of *CHEK2:p.K373E* + *MRE11A:p.K464R* and *MRE11A:p.K464R* + *CHEK2:p.R406H* in post-treatment in patients' PFS. The results showed they significantly reduced the survival benefits of patients (Figure 5M,N, Table S4). Furthermore, the combined three mutation sites also highlighted the negative impact on patients' prognosis (Figures S4E and S5, Table S4). In addition, we analyzed the effects of mutations or newly acquired mutations in *MRE11A:p.K464R*, *CHEK2:p.R474C*, *PIK3CA:p.E707K*, *ATM:p.I1407T*, and *CHEK2:p.Y390C* on patients' prognosis (Figure S6A–G). However, no meaningful results were observed.

Compared with single-mutation sites, we were surprised to find that, except for *MRE11A:p.K464R* + *CHEK2:p.R406H*, combined mutation sites did not improve the efficiency of prognostic assessment in patients, especially when compared with *MRE11A:p.K464R* or *CHEK2:p.R406H* (Figures 5M,N, S4C–E, and S6H,I). By analyzing the characteristics of mutation sites, we found that variations of *CHEK2:p.K373E* and *CHEK2:p.R406H* came from dynamic fluctuations of content during olaparib treatment. Increased *CHEK2:p.K373E* and *CHEK2:p.R406H* often predicted a poor prognosis, suggesting that they had great potential as monitoring indicators for olaparib maintenance therapy. Interestingly, newly acquired *MRE11A:p.K464R* was often accompanied by relapse (6/13) or subsequent short-term disease progression (6/13), indicating that it could be a vital driving factor for olaparib resistance in patients (Figure 5K) and is expected to be a reliable indicator and intervention target for olaparib resistance. Encouragingly, compared with CA125, it was further confirmed that the fluctuations of *CHEK2:p.K373E*, *CHEK2:p.R406H*, and *MRE11A:p.K464R* were in good agreement with CA125, and had a good potential for clinical transformation (Figure S7).

In conclusion, we found that mutation profiles in cfDNA can be used for efficacy evaluation and resistance monitoring in HGSOC patients with olaparib maintenance therapy. Our results will contribute to constructing clinical prediction models of olaparib treatment, guide the formulation of combination therapy after olaparib resistance, and optimize the clinical application of PARPi. In addition, the discovery of *MRE11A:p.K464R* will provide a focus for developing targeted drugs and will promote the progress of diagnosis and treatment of ovarian cancer.

4 | DISCUSSION

In our study, we examined the possibility of mutation profiles in cfDNA as a predictive biomarker for responses and outcomes of olaparib maintenance therapy. Platinum-sensitive HGSOC patients who had a relapse and were scheduled to receive olaparib maintenance therapy were enrolled.

In recent years, cfDNA analysis as a noninvasive detection technology has been widely used in clinical practice, such as noninvasive prenatal testing, organ transplantation monitoring, and cancer fluid biopsy.[12] Genomic or epigenomic alterations of cells can be analyzed by cfDNA detection, including point mutations,[16] copy number alterations,[25] and methylation changes.[26] In addition, cfDNA can also be used to detect exosomal DNA, chromosomal rearrangements, and viral or bacterial DNA fragments in plasma.[27,28] For ovarian cancer studies, cfDNA analysis can be used to undertake a comprehensive molecular analysis of tumors,[29–31] such as *BRCA* reversion mutations and copy-number alterations. This evidence indicates that it is theoretically feasible to solve the clinical dilemma of olaparib resistance by cfDNA analysis. However, previous cfDNA studies mainly focused on tumor characteristics and *BRCA* variations, and explored their associations with patients' prognosis.[18,32–34] Previous studies ignored the critical role of whole mutation profiles in PARPi treatment and lacked the specific and universal indicators of PARPi resistance. To our knowledge, our work represents the most comprehensive study of cfDNA mutation profiles before and after olaparib treatment in relapsed HGSOC patients, identifying the associations between somatic mutation sites and olaparib resistance.

Here, we undertook personalized cfDNA detection using CLAmp-seq to determine mutation profiles of each patient. We found that increased Max MAF in post-treatment predicted a poor prognosis (Figure 2) and patients with pathogenic germline mutations in the HRR pathway had significantly superior PFS compared with negative ones (Figure 3). In addition, we also observed that *MRE11A:p.K464R* under pathogenic germline mutations was associated with shortened PFS, which has not been reported in relevant ovarian cancer studies (Figure S2L). If validated by further studies, this finding could profoundly influence the olaparib treatment in HGSOC patients with pathogenic gBRCA mutations.

Recent studies have shown that somatic mutations in cfDNA are closely related to drug resistance in patients.[16,35,36] We speculate that somatic mutations will be more promising to screen the universal indicators for olaparib resistance. In our results, new somatic mutations in post-treatment predict a poor prognosis, and the larger proportion of new mutation load, the worse the patients' prognosis (Figure 4E). Furthermore, we unexpectedly found that *MRE11A* mutations in pretreatment and post-treatment could both effectively differentiate the prognosis of patients, but their effects on prognosis were completely opposite. In the subsequent analyses, we found that *MRE11A* mutations mainly came from *MRE11A:p.K464R* (17/18). This is an interesting phenomenon worthy of further study. MRE11A, as an important component of the MRE11A–RAD50–NBS1 complex, plays a crucial role in DDR.[37,38] In addition, MRE11A is involved in cellular bioenergetic regulation, protecting the mitochondria and

FIGURE 5 Associations between somatic mutation sites and the prognosis of olaparib maintenance therapy in patients with high-grade serous ovarian carcinoma. (A, B) Distribution maps of somatic mutation sites in pretreatment (A) and post-treatment (B) patients. (C–E) Survival analyses of *CHEK2:p.K373E* (C, $p = 0.0219$), *CHEK2:p.R406H* (D, $p = 0.1319$), and *MRE11A:p.K464R* (E, $p = 0.0267$) in pretreatment. (F, G) Mutation (mut) tracking of *CHEK2:p.K373E* (F) and *CHEK2:p.R406H* (G) in cell-free DNA (cfDNA) detection during olaparib treatment. (H, I) Survival analyses of *CHEK2:p.K373E*-higher (H, $p = 0.0091$) and *CHEK2:p.R406H*-higher (I, $p = 0.0002$) in post-treatment. (J) Mutation tracking of *MRE11A:p.K464R* in cfDNA detection during olaparib treatment. (K) Longitudinal representation of *MRE11A:p.K464R* from all patients with a timepoint available. (L) Survival analysis of newly acquired *MRE11A:p.K464R* (G, $p = 0.0005$) in post-treatment. (M, N) Survival analyses of combined somatic mutation sites of post-*CHEK2:p.K373E* + post-*MRE11A:p.K464R* (M, $p = 0.0120$) and post-*MRE11A:p.K464R* + post-*CHEK2:p.R406H* (N, $p < 0.0001$) in patients. HR, hazard ratio; mPFS, median PFS; PARPi, poly(ADP-ribose) polymerase inhibitor

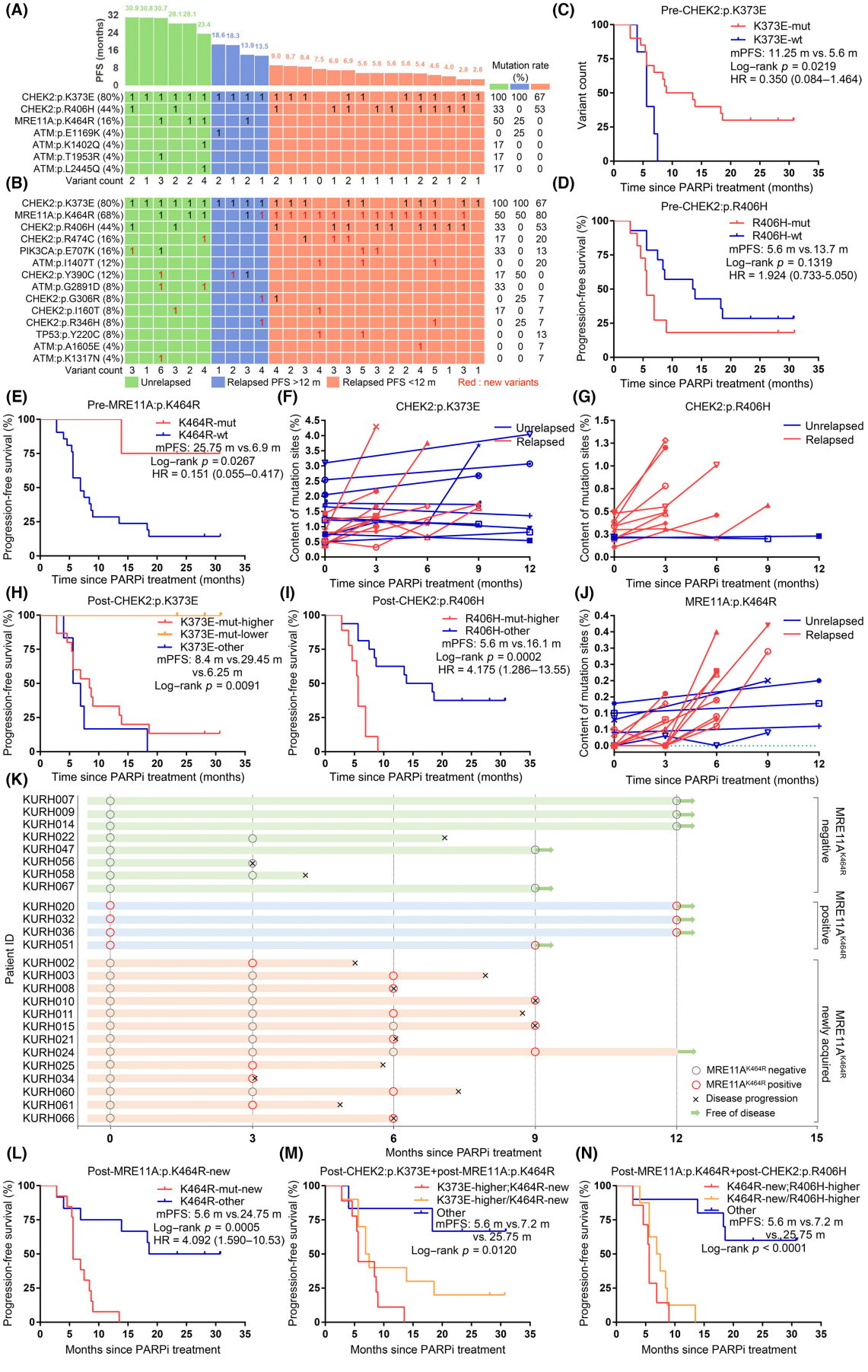
(A)
PFS (months)
Mutation rate (%)
CHEK2:p.K373E (80%)
CHEK2:p.R406H (44%)
MRE11A:p.K464R (16%)
ATM:p.E1169K (4%)
ATM:p.K1402Q (4%)
ATM:p.T1953R (4%)
ATM:p.L2445Q (4%)
Variant count
(B)
CHEK2:p.K373E (80%)
MRE11A:p.K464R (68%)
CHEK2:p.R406H (44%)
CHEK2:p.R474C (16%)
PIK3CA:p.E707K (16%)
ATM:p.I1407T (12%)
CHEK2:p.Y390C (12%)
ATM:p.G2891D (8%)
CHEK2:p.G306R (8%)
CHEK2:p.I160T (8%)
CHEK2:p.R346H (8%)
TP53:p.Y220C (4%)
ATM:p.A1605E (4%)
ATM:p.K1317N (4%)
Variant count
Unrelapsed
Relapsed PFS >12 m
Relapsed PFS <12 m
Red : new variants
(C)
Pre-CHEK2:p.K373E
K373E-mut
K373E-wt
mPFS: 11.25 m vs. 5.6 m
Log–rank p = 0.0219
HR = 0.350 (0.084–1.464)
Variant count
Time since PARPi treatment (months)
(D)
Pre-CHEK2:p.R406H
R406H-mut
R406H-wt
mPFS: 5.6 m vs.13.7 m
Log–rank p = 0.1319
HR = 1.924 (0.733-5.050)
Progression-free survival (%)
Time since PARPi treatment (months)
(E)
Pre-MRE11A:p.K464R
K464R-mut
K464R-wt
mPFS: 25.75 m vs.6.9 m
Log–rank p = 0.0267
HR = 0.151 (0.055–0.417)
Progression-free survival (%)
Time since PARPi treatment (months)
(F)
CHEK2:p.K373E
Unrelapsed
Relapsed
Content of mutation sites (%)
Time since PARPi treatment (months)
(G)
CHEK2:p.R406H
Unrelapsed
Relapsed
Content of mutation sites (%)
Time since PARPi treatment (months)
(H)
Post-CHEK2:p.K373E
K373E-mut-higher
K373E-mut-lower
K373E-other
mPFS: 8.4 m vs.29.45 m vs.6.25 m
Log–rank p = 0.0091
Progression-free survival (%)
Time since PARPi treatment (months)
(I)
Post-CHEK2:p.R406H
R406H-mut-higher
R406H-other
mPFS: 5.6 m vs.16.1 m
Log–rank p = 0.0002
HR = 4.175 (1.286–13.55)
Progression-free survival (%)
Time since PARPi treatment (months)
(J)
MRE11A:p.K464R
Unrelapsed
Relapsed
Content of mutation sites (%)
Time since PARPi treatment (months)
(K)
Patient ID
KURH007
KURH009
KURH014
KURH022
KURH047
KURH056
KURH058
KURH067
KURH020
KURH032
KURH036
KURH051
KURH002
KURH003
KURH008
KURH010
KURH011
KURH015
KURH021
KURH024
KURH025
KURH034
KURH060
KURH061
KURH066
MRE11A^K464R negative
MRE11A^K464R positive
Disease progression
Free of disease
MRE11A^K464R negative
MRE11A^K464R positive
MRE11A^K464R newly acquired
Months since PARPi treatment
(L)
Post-MRE11A:p.K464R-new
K464R-mut-new
K464R-other
mPFS: 5.6 m vs.24.75 m
Log–rank p = 0.0005
HR = 4.092 (1.590–10.53)
Progression-free survival (%)
Months since PARPi treatment
(M)
Post-CHEK2:p.K373E+post-MRE11A:p.K464R
K373E-higher;K464R-new
K373E-higher/K464R-new
Other
mPFS: 5.6 m vs.7.2 m vs. 25.75 m
Log–rank p = 0.0120
Progression-free survival (%)
Months since PARPi treatment
(N)
Post-MRE11A:p.K464R+post-CHEK2:p.R406H
K464R-new;R406H-higher
K464R-new/R406H-higher
Other
mPFS: 5.6 m vs.7.2 m vs. 25.75 m
Log–rank p < 0.0001
Progression-free survival (%)
Months since PARPi treatment

preventing T cell pyroptosis.[39] Therefore, we speculate that the balance of biological functions of MRE11A is disrupted in olaparib treatment, leading to the opposite prognostic effects. In brief, patients with *MRE11A:p.K464R* in pretreatment have more stable cellular bioenergetic regulation and more vigorous immune microenvironment, which improve the survival benefits of patients. After olaparib treatment, newly acquired *MRE11A:p.K464R* combined with accumulated DNA damage highlight the DDR function of MRE11A, leading to olaparib resistance. Of course, further research is needed to verify our speculation. In addition, we observed that *CHEK2:p.K373E* and *CHEK2:p.R406H* were strongly correlated with patients' PFS, which could be used for efficacy evaluation of olaparib.

For the system of cfDNA analysis, CLAmp-seq has the following advantages. Our detection was based on high-throughput sequencing with extremely high efficiency compared with droplet digital PCR or BEAMing (beads, emulsion, amplification, magnetics digital PCR).[40] Moreover, due to low content of cfDNA, low-frequency mutations. and rare mutations, the sensitivity of detection technology was greatly challenged,[41–44] such as NGS or cancer personalized profiling by deep sequencing (CAPP-Seq). The CLAmp-seq method can achieve accurate and specific amplification of cfDNA by applying the strategy of "single chain loopization and concatemer error correction,"[22] with higher accuracy and reliability. We also filtered the sequencing data using clonal hematopoietic mutations of WBC[45–47] to avoid the false positives before undertaking the cfDNA mutation analysis.

Inevitably, our cfDNA analysis did have certain limitations, including the inability to define the evolution profiles of existing mutations in the course of treatment, to detect new second primary cancers or identify cancer metastasis.[48] Moreover, due to the short length and low content of tumor-derived DNA fragments, it is easy to lead to false negative results. Therefore, cfDNA detection techniques need to be further optimized to continuously improve the threshold of variant detection. However, new therapeutic strategies based on our findings could be developed in future clinical studies. For example, olaparib can be actively given to patients with *MRE11A:p.K464R* in pretreatment. Noncarriers can dynamically monitor *MRE11A:p.K464R* by cfDNA detection, providing early warning for olaparib resistance. Further studies in larger cohorts are warranted to validate the role of *MRE11A:p.K464R* in olaparib treatment due to the limitation of sample size in this study.

In summary, dynamic analyses of mutation profiles in cfDNA could facilitate the timely adjustment of treatment strategies and improve the survival benefits of HGSOC patients with olaparib maintenance therapy. The discovery of *MRE11A:p.K464R* will not only provide a complementary or alternative indicator for diagnosis and treatment of ovarian cancer but also provide a focus for targeted drugs, and lay the theoretical basis for the development of combination therapy after olaparib resistance.

ACKNOWLEDGMENTS

We thank AccuraGen Biotechnology Co., Ltd for excellent technical help, and the donors who participated in this study. This study was supported by the National Natural Science Foundation of China (81874106, 81974408, 82073259, and 82103065), the Key Research and Development Program of Hubei Province (2020BCA067), and the Hubei Province Science Fund for Distinguished Young Scholars (2020CFA066).

CONFLICT OF INTEREST

The authors have no conflict of interest.

DATA AVAILABILITY STATEMENT

The data that support the findings of this study are openly available in the European Nucleotide Archive.

ETHICS STATEMENT

The study was approved by the Ethics Committee of Tongji Hospital, Tongji Medical College, Huangzhong University of Science and Technology. Study subjects provided informed consent to allow the collection of blood and analysis of clinical and genetic data for this work.

ORCID

Junpeng Fan https://orcid.org/0000-0002-9413-408X
Xue Wu https://orcid.org/0000-0001-6793-9918
Chaoyang Sun https://orcid.org/0000-0003-2469-1638

REFERENCES

1. Lheureux S, Braunstein M, Oza AM. Epithelial ovarian cancer: evolution of management in the era of precision medicine. *CA Cancer J Clin*. 2019;69:280-304.
2. Li H, Liu ZY, Wu N, Chen YC, Cheng Q, Wang J. PARP inhibitor resistance: the underlying mechanisms and clinical implications. *Mol Cancer*. 2020;19:107.
3. Curtin NJ, Szabo C. Poly(ADP-ribose) polymerase inhibition: past, present and future. *Nat Rev Drug Discov*. 2020;19:711-736.
4. Armstrong DK, Alvarez RD, Bakkum-Gamez JN, et al. Ovarian cancer, version 2.2020, NCCN clinical practice guidelines in oncology. *J Natl Compr Cancer Netw*. 2021;19:191-226.
5. Tew WP, Lacchetti C, Ellis A, et al. PARP inhibitors in the management of ovarian cancer: ASCO guideline. *J Clin Oncol*. 2020;38:3468-3493.
6. Warner E, Herberts C, Fu S, et al. BRCA2, ATM, and CDK12 defects differentially shape prostate tumor driver genomics and clinical aggression. *Clin Cancer Res*. 2021;27:1650-1662.
7. Noordermeer SM, van Attikum H. PARP inhibitor resistance: a tug-of-war in BRCA-mutated cells. *Trends Cell Biol*. 2019;29:820-834.
8. Cruz C, Castroviejo-Bermejo M, Gutiérrez-Enríquez S, et al. RAD51 foci as a functional biomarker of homologous recombination repair and PARP inhibitor resistance in germline BRCA-mutated breast cancer. *Ann Oncol*. 2018;29:1203-1210.
9. Goodall J, Mateo J, Yuan W, et al. Circulating cell-free DNA to guide prostate cancer treatment with PARP inhibition. *Cancer Discov*. 2017;7:1006-1017.
10. Sun C, Fang Y, Yin J, et al. Rational combination therapy with PARP and MEK inhibitors capitalizes on therapeutic liabilities in RAS mutant cancers. *Sci Transl Med*. 2017;9(392):eaal5148.
11. Campos-Carrillo A, Weitzel JN, Sahoo P, et al. Circulating tumor DNA as an early cancer detection tool. *Pharmacol Ther*. 2020;207:107458.
12. Wan JCM, Massie C, Garcia-Corbacho J, et al. Liquid biopsies come of age: towards implementation of circulating tumour DNA. *Nat Rev Cancer*. 2017;17:223-238.

13. Cheng ML, Pectasides E, Hanna GJ, Parsons HA, Choudhury AD, Oxnard GR. Circulating tumor DNA in advanced solid tumors: clinical relevance and future directions. *CA Cancer J Clin*. 2021;71:176-190.
14. Chen G, Peng J, Xiao Q, et al. Postoperative circulating tumor DNA as markers of recurrence risk in stages II to III colorectal cancer. *J Hematol Oncol*. 2021;14:80.
15. Lam VK, Zhang J, Wu CC, et al. Genotype-specific differences in circulating tumor DNA levels in advanced NSCLC. *J Thorac Oncol*. 2021;16:601-609.
16. Ortiz-Cuaran S, Mezquita L, Swalduz A, et al. Circulating tumor DNA genomics reveal potential mechanisms of resistance to BRAF-targeted therapies in patients with BRAF-mutant metastatic non-small cell lung cancer. *Clin Cancer Res*. 2020;26:6242-6253.
17. Tukachinsky H, Madison RW, Chung JH, et al. Genomic analysis of circulating tumor DNA in 3,334 patients with advanced prostate cancer identifies targetable BRCA alterations and AR resistance mechanisms. *Clin Cancer Res*. 2021;27:3094-3105.
18. Lin KK, Harrell MI, Oza AM, et al. BRCA reversion mutations in circulating tumor DNA predict primary and acquired resistance to the PARP inhibitor rucaparib in high-grade ovarian carcinoma. *Cancer Discov*. 2019;9:210-219.
19. Faust GG, Hall IM. SAMBLASTER: fast duplicate marking and structural variant read extraction. *Bioinformatics (Oxford, England)*. 2014;30:2503-2505.
20. Garrison E, Marth G. Haplotype-based variant detection from short-read sequencing. *arXiv*. 2012. doi:10.48550/arXiv.1207.3907
21. Paila U, Chapman BA, Kirchner R, Quinlan AR. GEMINI: integrative exploration of genetic variation and genome annotations. *PLoS Computat Biol*. 2013;9:e1003153.
22. Wang L, Hu XM, Guo QM, et al. CLAmp-seq: a novel amplicon-based NGS assay with concatemer error correction for improved detection of actionable mutations in plasma cfDNA from patients with NSCLC. *Small Methods*. 2019;4:1900357.
23. Osumi H, Shinozaki E, Takeda Y, et al. Clinical relevance of circulating tumor DNA assessed through deep sequencing in patients with metastatic colorectal cancer. *Cancer Med*. 2019;8:408-417.
24. An Y, Guan Y, Xu Y, et al. The diagnostic and prognostic usage of circulating tumor DNA in operable hepatocellular carcinoma. *Am J Transl Res*. 2019;11:6462-6474.
25. Paracchini L, Beltrame L, Grassi T, et al. Genome-wide copy-number alterations in circulating tumor DNA as a novel biomarker for patients with high-grade serous ovarian cancer. *Clin Cancer Res*. 2021;27:2549-2559.
26. Luo H, Wei W, Ye Z, Zheng J, Xu RH. Liquid biopsy of methylation biomarkers in cell-free DNA. *Trends Mol Med*. 2021;27:482-500.
27. Snyder MW, Kircher M, Hill AJ, Daza RM, Shendure J. Cell-free DNA comprises an in vivo nucleosome footprint that informs its tissues-of-origin. *Cell*. 2016;164:57-68.
28. Stewart CM, Kothari PD, Mouliere F, et al. The value of cell-free DNA for molecular pathology. *J Pathol*. 2018;244:616-627.
29. Vitale SR, Groenendijk FH, van Marion R, et al. TP53 mutations in serum circulating cell-free tumor DNA as longitudinal biomarker for high-grade serous ovarian cancer. *Biomolecules*. 2020;10:415.
30. Stamenkovic S, Cheng J, Surowy H, Burwinkel B, Gündert M. Circulating cell-free DNA variables as marker of ovarian cancer patients: a pilot study. *Cancer Biomark*. 2020;28:159-167.
31. Widschwendter M, Zikan M, Wahl B, et al. The potential of circulating tumor DNA methylation analysis for the early detection and management of ovarian cancer. *Genome Med*. 2017;9:116.
32. Rusan M, Andersen RF, Jakobsen A, Steffensen KD. Circulating HOXA9-methylated tumour DNA: A novel biomarker of response to poly (ADP-ribose) polymerase inhibition in BRCA-mutated epithelial ovarian cancer. *Eur J Cancer (Oxford, England : 1990)*. 2020;125:121-129.
33. Noguchi T, Iwahashi N, Sakai K, et al. Comprehensive gene mutation profiling of circulating tumor DNA in ovarian cancer: its pathological and prognostic impact. *Cancers*. 2020;12:3382.
34. Van Berckelaer C, Brouwers AJ, Peeters DJ, Tjalma W, Trinh XB, van Dam PA. Current and future role of circulating tumor cells in patients with epithelial ovarian cancer. *Eur J Surg Oncol*. 2016;42:1772-1779.
35. Yen I, Shanahan F, Lee J, et al. ARAF mutations confer resistance to the RAF inhibitor belvarafenib in melanoma. *Nature*. 2021;594:418-423.
36. Subbiah V, Shen T, Terzyan SS, et al. Structural basis of acquired resistance to selpercatinib and pralsetinib mediated by non-gatekeeper RET mutations. *Ann Oncol*. 2021;32:261-268.
37. Tisi R, Vertemara J, Zampella G, Longhese MP. Functional and structural insights into the MRX/MRN complex, a key player in recognition and repair of DNA double-strand breaks. *Computat Struct Biotechnol J*. 2020;18:1137-1152.
38. Bian L, Meng Y, Zhang M, Li D. MRE11-RAD50-NBS1 complex alterations and DNA damage response: implications for cancer treatment. *Mol Cancer*. 2019;18:169.
39. Li Y, Shen Y, Jin K, et al. The DNA repair nuclease MRE11A functions as a mitochondrial protector and prevents T cell pyroptosis and tissue inflammation. *Cell Metab*. 2019;30:477-492.e476.
40. Buono G, Gerratana L, Bulfoni M, et al. Circulating tumor DNA analysis in breast cancer: is it ready for prime-time? *Cancer Treat Rev*. 2019;73:73-83.
41. Mauger F, Horgues C, Pierre-Jean M, Oussada N, Mesrob L, Deleuze JF. Comparison of commercially available whole-genome sequencing kits for variant detection in circulating cell-free DNA. *Sci Rep*. 2020;10:6190.
42. Lam SN, Zhou YC, Chan YM, et al. Comparison of target enrichment platforms for circulating tumor DNA detection. *Sci Rep*. 2020;10:4124.
43. Oreskovic A, Brault ND, Panpradist N, Lai JJ, Lutz BR. Analytical comparison of methods for extraction of short cell-free DNA from urine. *J Mol Diagn*. 2019;21:1067-1078.
44. Ignatiadis M, Sledge GW, Jeffrey SS. Liquid biopsy enters the clinic - implementation issues and future challenges. *Nat Rev Clin Oncol*. 2021;18:297-312.
45. Jensen K, Konnick EQ, Schweizer MT, et al. Association of clonal hematopoiesis in DNA repair genes with prostate cancer plasma cell-free DNA testing interference. *JAMA Oncol*. 2021;7:107-110.
46. Chan HT, Nagayama S, Chin YM, et al. Clinical significance of clonal hematopoiesis in the interpretation of blood liquid biopsy. *Mol Oncol*. 2020;14:1719-1730.
47. Razavi P, Li BT, Brown DN, et al. High-intensity sequencing reveals the sources of plasma circulating cell-free DNA variants. *Nat Med*. 2019;25:1928-1937.
48. Begg CB, Ostrovnaya I, Geyer FC, et al. Contralateral breast cancers: independent cancers or metastases? *Int J Cancer*. 2018;142:347-356.

SUPPORTING INFORMATION

Additional supporting information can be found online in the Supporting Information section at the end of this article.

How to cite this article: Hu D, Guo E, Yang B, et al. Mutation profiles in circulating cell-free DNA predict acquired resistance to olaparib in high-grade serous ovarian carcinoma. *Cancer Sci*. 2022;113:2849-2861. doi: 10.1111/cas.15456